Stream response to precipitation variability: a spectral view based on analysis and modeling of hydrological cycle components

D. Markovic[1,2*], M. Koch[1]

[1]Department of Geohydraulics and Engineering Hydrology, University of Kassel, Kurt Woltersstr. 3, 34109 Kassel, Germany

[2]Leibniz-Institute of Freshwater Ecology and Inland Fisheries, Müggelseedamm 310, 12587 Berlin, Germany

Abstract:

Hydrological processes commonly exhibit long-term persistence, also known as the "Hurst phenomenon". Here we examine long-term precipitation and streamflow time series from the Elbe River Basin to quantify differences in the spectral properties and in the Hurst parameter estimates ($\hat{H}$) of the individual hydrological cycle components. Precipitation-runoff modeling is performed for the Elbe River sub-catchment Strigies using the Soil and Water Assessment Tool (SWAT). For 38 daily 50 years long streamflow time series from the Elbe River Basin, baseflow separation and spectral analysis is performed. The results show a spectral shift towards low-frequency scales (>2 yr.) from precipitation to baseflow, with a parallel increase of $\hat{H}$ from 0.52 (precipitation) to 0.65 (baseflow). The SWAT model is able to reproduce both, the main low-frequency mode (≈7 yr.) and the $\hat{H}$ (0.62) of the observed Striegis River flow time series. The baseflow appears to be the main component which shapes the low-frequency response and $\hat{H}$ of streamflow in the Elbe River Basin to the input precipitation. This conclusion is further confirmed through PMWIN-MODFLOW groundwater-modeling of a hypothetic phreatic stream-connected aquifer system that consists of various soils (sand, loamy sand and silt). A power shift towards lower frequencies and an increase of $\hat{H}$ for the hydraulic heads is obtained, as the aquifer's lateral dimensions increase and its hydraulic conductivity decreases. The average $\hat{H}$ of the groundwater heads is 0.80, 0.91 and 1.0 for sand-, loamy sand- and silt-aquifer, respectively.

KEY WORDS, Hurst parameter, persistence, Elbe River, hydrological cycle components, baseflow, groundwater modeling

Short title: Basin low frequency response to precipitation forcing

INTRODUCTION

Stream response to precipitation variability results from the passage of infiltrated water through several subsurface filters that, depending on the scale range, have the effect to either amplify or attenuate the precipitation's variability modes (cf. Shun and Duffy 1999). Consequently, the output signal - the streamflow-, can have significantly different spectral

*Correspondence to: Danijela Markovic, Leibniz-Institute of Freshwater Ecology and Inland Fisheries, Müggelseedamm 310, 12587 Berlin, Germany.
E-mail: markovic@igb-berlin.de

characteristics than the input signal - the precipitation. Particular stages of the hydrological cycle such as the interception and the evapotranspiration may lead to a reduction of the precipitation's high frequency variability, while snow melting produces the opposite effect (cf. Milly and Wetherald, 2002). Moreover, the groundwater aquifer may behave like a fractal frequency filter, resulting in temporal scaling of hydraulic head fluctuations and of baseflow (Zhang and Schilling, 2004). For example, using a linear- reservoir model with a white-noise recharge input, Zhang and Li (2005) showed that the simulated hourly hydraulic head fluctuations over 4 years long period for homogenous and heterogeneous aquifers are characterized by a Hurst parameter of $H = 0.42$.

In fact, the Hurst parameter is commonly used an indicator of the time series' long-range memory, i.e., persistence (Beran, 1994; Koutsoyiannis, 2005a, 2005b, 2008). For $0 < H < 0.5$ the process has short-term persistence, for $H = 0.5$ the observations are uncorrelated and for $0.5 < H < 1$ the process has long-term persistence. Hydrological processes are generally considered to exhibit long-term persistence, also known as the "Hurst phenomenon" (Lohre et al, 2003; Koutsoyiannis et al., 2008). For example, using spectral or time-domain time series methods, the H parameter of the Columbia River has been estimated as H =0.85 (Villarini et al. 2009), the Boeoticos Kephisos river flows as H=0.79 (Koutsoyiannis, 2006), the annual Nile river flow as H=0.85 (Koutsoyiannis *et al*., 2008), and for the Elbe River flow at Neu Darchau as H= 0.80 (Markovic and Koch, 2013).

There have been numerous attempts to explain the "Hurst phenomenon" from statistical and physical points of view (see e.g. Koutsoyiannis, 2008; Koutsoyiannis, 2011). However, finding of a convincing physical explanation is rather difficult, since even short-term persistence can induce pre-asymptotic behaviour, resulting in H parameter estimates above 0.5, especially, when dealing with time-limited series (Montanari, 2003).

Unlike the spectra of streamflow time series commonly characterised by H>0.5, precipitation spectra are often characterised by $H \approx 0.50$ (Markovic and Koch, 2013). The differences in the Hurst parameter estimates between precipitation and streamflow has been argued by Koutsoyiannis (2006) by an increased complexity of the system which causes more Hurst-like growth of the system's output. An interesting issue is then the spectral transformation of the input signal-precipitation through the hydrological cycle. Precipitation spectrum is often characterized by peaks at characteristic interannual to interdecadal scales due to large-scale climate patterns like the North Atlantic Oscillation (NAO) and the Arctic oscillation (AO) (Ionita et al., 2011). However, though apparent, the issue of interannual to interdecadal or even longer cycles in hydrological time series due to large scale climate variability is commonly omitted in analyses of the series' Hurst parameter (but see Markonis and Koutsoyiannis, 2013; Markovic and Koch, 2013). The presence of such components in the time series can significantly affect the H parameter estimates, such that $H \gg 0.5$, i.e. long-term persistence is deduced (Montanari *et al.*, 1999; Markovic and Koch, 2005). An additional effect that needs consideration when addressing the H of the streamflow time series is the strengthening of the climate signal at the interannual and decadal scales for groundwater-dominated streamflow time series (see Shun and Duffy, 1999). Therefore, we argue that the question of long-range memory of streamflow time series reported for many streams in recent years (e.g. Markovic and Koch, 2013; Koutsoyiannis, 2005a, 2005b, 2008; Lohre et al., 2003) has to be readdressed in terms of the low-frequency variability of the hydrological cycle components.

The primary objective of this study is to follow the journey of the low-frequency climate signal through the hydrological cycle and study its role on the Hurst parameter estimates of the individual hydrological cycle components. Through deterministic, integrated surface-groundwater modeling combined with stochastic time series analysis, the changes in the low frequency components and Hurst parameter estimates of all relevant processes that lead to streamflow generation will be studied. In particular, the water movement through the

hydrological cycle, which starts with precipitation and, after going through the processes of evapotranspiration, direct flow, soil water infiltration, groundwater recharge, ends its "journey" as baseflow in the main stream, will be simulated for the Striegis River Basin with the Soil and Water Assesment Tool (SWAT) (Neitsch *et al.*, 2011). Furthermore, for 38 daily streamflow time series observed over the time interval 1951-2000, baseflow separation and analyses of the scaling properties of the hydrological cycle components will be performed. Using the well-known MODFLOW groundwater model (Harbaugh and McDonald, 1996), as embedded in the PMWIN package (Chiang and Kinzelbach, 2005), we will examine the role of the aquifer in the transport of the low frequency climate signal towards the connected stream. Specifically, the main aims of this study are: (1) to identify changes in the low-frequency variability and the Hurst parameter estimates across the individual hydrological cycle components in the Striegis River Basin; (2) to compare the Hurst parameter estimates of the long-term base-, direct- and total flows across the Elbe River Basin and (3) to investigate the connection between the long-term persistence (H>0.5) of the river flows, and the processes involved in the transformation of the input basin signal - the precipitation - to the output signal- the streamflow, for the various aquifer types (sand-, loamy sand- and silt aquifers).

STUDY AREA AND DATA

The overall study area is the German part of the Elbe River Basin (Figure 1), with a drainage area of 96400 km^2 which is about two thirds of its total basin size (147800 km^2). The streamflow data base consists of 38 continuous time series observed at gauges all over the Elbe River Basin over the time interval January 1951- December 2000. The long-term streamflow in the sub-basins ranges between 100 and 300 mm/y which is to be compared with an average annual basin precipitation of about 715 mm.

For the climate gages indicated in Figure 1, the German National Meteorological Service (DWD) provided continuous (1951-2000) daily measurements of the following variables: temperature, precipitation, humidity, air pressure, vapor pressure, hours of bright sunshine, degree of cloud cover, short wave radiation and wind speed. The soil, the land use and the DEM data were provided by the Saxon State Office for Environment and Geology, the German Federal Statistical Office and the Potsdam Institute for Climate Impact Research, respectively.

The process-based SWAT model was implemented in the Striegis River catchment (Figure 1). The Striegis River originates at the confluence of the Große Striegis and Kleine Striegis River, with the catchment area defined from there of about 283 km^2, and a maximum elevation difference of 400 m. At the gage Niederstriegis, located 200 m upstream of the Striegis River mouth to the Freiberger Mulde River, the average long-term (1951-2000) measured daily flow is 2.8 m^3/s. The average annual catchment precipitation is 780 mm and the average annual runoff at the basin outlet amounts to 330 mm. More than 75% of the catchment is agricultural land, about 10% is covered by evergreen forest and about 6.3% by med/low density residential areas. For more than 80% of the catchment, the soil conductivity is classified as very low ($10^{-9} - 10^{-7}$ m/s) to low ($10^{-7} - 10^{-5}$ m/s) (HÜK 200, 2005).

METHODS

Theoretical background of the study

Short summer rain events in the northern hemisphere's mid-latitudes usually do not cause groundwater recharge, implying that the piezometric heads are not affected by such triggering

surface events as these act only on a short time scale. On the other hand, groundwater heads reflect the effects of annual and, of course, interannual weather pattern changes with periods of "wet" or "dry" years, triggered, for example, by NAO and AO (cf. Markovic and Koch, 2013). Short-period (e.g. daily) variations only propagate into the upper "skin" of the earth ("skin-effect"), while the long-period oscillations such as those due to the e.g. NAO or AO penetrate deeper into the earth's crust (see Shun and Duffy, 1999).

Although obvious, the "skin-effect" issue has been until now overlooked in the studies of "Hurst phenomenon" in discharge series. Therefore, a brief mathematical explanation of the role of "skin-effect" in transport of the low frequency signals in hydrological processes will be given. Mathematically, the skin-effect is a consequence of the parabolic nature of the diffusion-like PDE. In the present application of groundwater hydrology the underlying PDE is the Richards equation (Richards, 1931) which describes the soil moisture, or water content, $\theta(z,t)$ as a function of (vertical) space z and time t and needs to be solved with the appropriate boundary condition (BC) $\theta(0,t)$ at the soil surface. For example, assuming a periodic input signal for the precipitation, the BC becomes $\theta(0,t) = A\cos(\omega t)$, with A, the amplitude; ω, the angular frequency = $2\pi f$, and assuming, to first order, $D = const.$ and $K = const.$, where D is the soil water diffusivity, and K the soil water conductivity, an analytical solution for $\theta(z,t)$ can be derived and written as (e.g Tikhonov and Samarski, 1960)

$$\theta(z,t) = A\, exp\left(-\sqrt{\frac{\omega}{2D}}\, z\right)\, cos\left(-\sqrt{\frac{\omega}{2D}}\, z + \omega t\right). \tag{1}$$

This equation shows that the amplitude of the input signal A decreases exponentially with depth z as $A(z) = A\, exp\left(-\sqrt{\frac{\omega}{2D}}\, z\right)$, whereby the decay factor is proportional to the signal frequency ω. Therefore, the cutoff-frequency (the highest signal frequency) decreases with depth implying that the groundwater recharge (water that reaches the groundwater level) will most probably have a colored spectrum.

Temporal scaling of groundwater head fluctuations for a known recharge spectrum have been studied by Gelhar (1993), Zhang and Schilling (2004), Zhang and Li (2005) and Schilling and Zhang (2012) for a stream-connected, phreatic aquifer. For such an aquifer, the rate of storage change can be related to the net recharge and the stream-aquifer inflow/outflow as

$$S\frac{dh}{dt} = W - a(h - h_0) \tag{2}$$

where S is the specific yield; h, the average groundwater head over the entire aquifer; h_0, the water level in the stream; W, the recharge rate; and a, the outflow constant defined as $a = \frac{3T}{L^2}$; with T, the transmissivity; and L, an appropriate length scale of the aquifer (Gelhar, 1993). The latter is related to the characteristic aquifer time scale t_c as $a = \frac{S}{t_c}$. Assuming a constant river stage (h_o) and a homogenous aquifer ($S, a = const$), Gelhar (1993) showed that the relationship between the power spectrum of the groundwater head fluctuations (S_{hh}) and the groundwater recharge (S_{ww}) is:

$$S_{hh} = \frac{S_{ww}}{a^2(1 + t_c^2\omega^2)} \tag{3}$$

Equation 3 states that the spectrum of the head is a result of a competitive relation between the geometric properties of the aquifer (a, S) and of the signal frequency $\omega = 2\pi f$. Since $t_c = \frac{S}{a}$, for a white noise S_{ww}, S_{hh} moves from a white toward a colored spectrum

when $t_c > \frac{1}{f}$. Furthermore, for a large L and small K, the first term of the denominator $\alpha^2 \to 0$, implying that for a white-noise recharge spectrum, the spectrum of the head S_{hh} will be proportional to f^{-2}. We remark here that the spectral exponent β is related to the Hurst exponent as β=2*H*-1 (Gilmore, 2002), implying *H*≈1.5. As mentioned in the introduction, Zhang and Li (2005) confirmed that a white-noise recharge indeed causes fractal hydraulic heads in both, homogenous and heterogeneous aquifers. However, they reported Hurst parameters between 0.51 and 0.57 for the observed- and between 0.41 and 0.42 for the simulated groundwater fluctuations. Since the aquifer is connected with a stream via the baseflow, the remaining question here is- what is the connection between $H \gg 0.5$ of the streamflow data and the spectral properties of the baseflow?

The baseflow contribution to the streamflow is closely related to the geological properties of the groundwater reservoir. In general, lateral groundwater flow to the stream in a stream-connected aquifer - which makes up the baseflow - is a consequence of an increase of the hydraulic gradient due to a recharge event. Assuming a homogenous, isotropic aquifer with time-constant physical properties, the groundwater flow Q_{gw} to the stream can be calculated from a standard analytical solution of the parabolic groundwater flow equation as (cf. Rorabaugh, 1964):

$$Q_{gw} = 2T\left(\frac{h_0}{L}\right) exp\left(-\frac{\pi^2 Tt}{4L^2 S}\right); \quad \frac{Tt}{L^2 S} > 0.2. \tag{4}$$

where h_0 is the stream water level height at time t_0. The exponent in Eq. 4 is known as the baseflow recession constant $\alpha = \frac{\pi^2 T}{4L^2 S}$, wherefore Eq. 4 can be expressed as:

$$Q_{gw} = 2T\left(\frac{h_0}{L}\right) exp(-\alpha t). \tag{5}$$

A comparison of the expressions for the baseflow recession constant (α) and of the characteristic aquifer time scale (t_c) leads to the conclusion that the relationship between the recharge- and the head spectrum can be retrieved from the streamflow hydrograph by

$$t_c = \frac{\pi^2}{12\alpha} = \frac{L^2 S}{3T}. \tag{6}$$

This confirms the necessity of a separate analysis of the streamflow basic components, namely, the direct flow and the baseflow, in order to understand the response of the streamflow to the input signal - the precipitation.

Deterministic models for surface- and groundwater flow simulation

For the examination of the hydrological cycle components in a Striegis River Basin the deterministic SWAT model (Neitsch *et al.*, 2011) was used. SWAT is a spatially distributed model that needs specific information on weather, topography, vegetation soil properties and land management practices in the basin. It is a continuous time model and enables the simulation of the long-term basin's response to arbitrary weather- and soil management conditions. The primary model outputs are the actual evapotranspiration, surface runoff, soil water changes, groundwater recharge, direct flow and the baseflow. For the automatic calibration of the various selected parameters we have coupled SWAT with the nonlinear parameter estimation program PEST (Doherty, 2009). Since the study focus is on long-term low frequency variability and Hurst parameter of the hydrological cycle components (> 1 yr.), we used monthly time steps within the SWAT calibration.

For the estimation of baseflow in basins, where the required input for physically based models is not available, two automated techniques for the analysis of the streamflow hydrograph are applied: BFI (IH, 1980) and the SWAT-BFI (Arnold *et al.*, 1995). The BFI method is based on the evaluation of the 5-days local minima, while the SWAT-BFI method

is based on the application of a recursive digital filter.

The MODFLOW finite difference model (McDonald and Harbaugh, 1988), as embedded in the PMWIN package (Chiang and Kinzelbach, 2005), is applied for the numerical simulation of the groundwater heads for a stream-connected hypothetical aquifer. Groundwater flow in a stream-connected phreatic aquifer can be described by combining Darcy's law with the continuity equation, resulting in the well-known nonlinear groundwater flow equation

$$\frac{\partial}{\partial x}\left(K\,h\frac{\partial h}{\partial x}\right) + R = S_y\frac{\partial h}{\partial t} \tag{7}$$

where h is the hydraulic head; K, the hydraulic conductivity; S_y, the specific yield; and R the time- dependent recharge from infiltrating soil water. Using Darcy's law, the groundwater flow Q_{gw} to the streamcan be estimated by calculating the hydraulic gradient between the river stage and the simulated, unknown hydraulic head in the first cell next to the river as $Q_{gw} = K\,L\,W\,\frac{h_0 - h}{M}$, where K is the hydraulic conductivity of the riverbed material. L- the length of the river within a cell, and W and M are the width and the thickness of the riverbed, respectively.

We used three aquifer types, namely sand, loamy sand and silt, with hydraulic conductivities of 7.1 m/d, 3.5 m/d and 0.06 m/d. For each of these three aquifer types, three different lateral dimensions of the aquifer are simulated: $L = 200$ m, 400 m and 800 m. As the study of Zhang and Li (2005) has shown that the heterogeneity of the aquifer has little effect on the scaling properties of the hydraulic head fluctuation, all aquifers are assumed here to be homogenous. Transient groundwater flow in a one-layer phreatic aquifer of varying thickness and horizontal size is simulated using a grid size of dx =1m, dy =1m and a stress period of one month, which is also the time increment of the forcing input recharge *R*. The latter is obtained from (1) the percolation (PERC) time series obtained with the SWAT model of the Striegis River Basin described above and (2) simulated white noise data ("numerical experiment"). For the hypothetic phreatic stream-connected aquifer we assumed a steep gradient towards the river (10 %), a specific yield of $S_y = 0.25$. As for the boundary conditions of the model, the left boundary is assumed to be the groundwater divide (i.e. no-flow) and the right boundary is set as a constant head boundary h at the stream, equal to the gage elevation in the stream.

Stochastic time series analysis methods

For the time series decomposition, the Singular Spectrum Analysis (SSA) method (Golyandina *et al.*, 2001; Ghil *et al.*, 2002) is used. The crucial step of the SSA method is singular value decomposition (SVD) of the L-lagged vectors of a time series. The main SSA parameter, the window width L, is set to ½ of the observation time period.

The spectral properties of the studied time series were identified using the continuous wavelet transform (Torrence and Compo, 1998). The wavelet transform is a common tool for performing a continuous time-frequency localization of a time series. The widely used Morlet wavelet is employed, with the non-dimensional frequency set to $\omega_0 = 6$. The global wavelet spectrum (GWS) representing the average of the wavelet power over all local wavelet spectra along the time axis and the normalized GWS (nGWS), (=GWS divided by the data variance σ_0^2) are computed. Following Torrence and Compo (1998), the statistical significance of the GWS is tested by the χ^2 - test against the hypothesis of red noise.

For the practical estimation of the Hurst parameter the Detrended Fluctuation Analysis (DFA) method (Peng *et al.*, 1994) is employed. In the initial step of the DFA method

accumulated time series are calculated by summing up the differences between the observed values ($x_i k$) and the series mean (μ): $y(i) = \sum_{k=1}^{i} (x_k - \mu)$. In the next step, the resulting series are split into non-overlapping segments of the length s, followed with series' detrending within each of these segments (done by subtracting the linear least square fit). The fluctuation function F(s) describes the segment's variance, and scales as $F(s) \sim s^H$, where *H* is the Hurst parameter.

RESULTS AND DISCUSSION

SWAT modeling of the mean monthly Striegis River flows

In the analysis of the results of the calibrated SWAT model using the full set of the available climate and streamflow data (1951-2000) the first two simulation years (1951-1952) were omitted, as these represent the usual intial spin-up of the hydrological system. Prior to the calibration, a sensitivity analysis (see White and Chaubey, 2005) was carried out to identify the most influential parameters in the SWAT model. These turned out to be the SCS curve number, the soil water available capacity AWC, the saturated hydraulic conductivity K, the baseflow recession constant α and the groundwater delay DELAY. The SCS curve number depends on the permeability of the soil, the land use and on the antecedent soil water conditions (Singh, 1992). The AWC is defined as the difference between the water content at field capacity and the water content at the permanent wilting point. The baseflow recession constant depends on the aquifer physical properties (see Eq. 4) and DELAY is the time-lag for the transfer of recharge water from the unsaturated soil profile into the shallow aquifer.

To overcome the deficits of the manual calibration of the most sensitive SWAT parameters, the nonlinear parameter estimation program PEST was integrated into the SWAT model (see also Wang and Brubaker, 2013). In contrast to the manually calibrated SWAT models, having coefficient of determination up to $R^2 = 0.44$, the automatic calibration model SWAT-PEST significantly improved the model performance, with $R^2 = 0.74$. Thus, over the investigated time period (1953-2000), the average simulated annual runoff (Q_{sim}), as well as the mean (μ) and standard deviation (Sx) of the monthly time series agree well with the corresponding measured data: $Q_{sim} = 328$ mm, $Q = 323$ mm; $\mu_{sim} = \frac{3.0m^3}{s}$, $\mu = \frac{2.9m^3}{s}$; $Sx_{sim} = \frac{2.33m^3}{,}$ $Sx = \frac{2.37m^3}{s}$. As Figure 2 shows, except for an overestimation of the observed flow extremes, there is an overall good agreement between the SWAT-PEST simulated- and the observed streamflows.

The normalized global wavelet spectra (nGWS) of the simulated hydrological cycle components for time-scales $s > 2$ yr. (Figure 3) indicate peaks at the ≈ 7 yr. and ≈ 10.4 yr. scales for all studied data except evapotranspiration. However, although prominent, these low frequency modes are not statistically significant at the 95 % significance level for none of the series. On the other hand, one apparent feature of nGWS's (Figure 3) is that the "journey" of water through the hydrological cycle, i.e., from the surface through the underground and back to the stream, is accompanied by an increase of power at low-frequency scales. As discussed in Markovic and Koch (2013), for much of the Elbe Basin, the source of such low-frequency oscillations are variability modes of large-scale oscillation patters, mainly the NAO and AO. Consequently, it is not surprising that the hydrological cycle components have increased power at similar low-frequency scales. In particular, except for a slight difference in the power at scales $s > 8$ yr., both the spectra of the direct flow component and of the percolation have almost the same shape as that of the basin precipitation. In line with the

theoretical expectations (see Eq. 1 and Gammaitoni *et al.*, 1998), the spectrum of the baseflow is characterised by a power shift towards low frequency scales. The comparison of the spectral power at the low frequency scales for the different hydrological cycle components (Figure 3), clearly reveals the dominant role of the baseflow in shaping the river flow's spectral response to the input signal, the precipitation. As a side remark, the contribution of the direct flow to the low-frequency part of the flow spectrum is negligible, compared with that of the baseflow.

Using the DFA method, the Hurst parameter of each of the simulated hydrological cycle components was estimated. The DFA method is known to be biased when a periodicity in the time series is present (Hu *et al.*, 2001; Markovic and Koch, 2013). This bias manifests itself by a tendency of obtaining small H for a time series with dominant high frequency (small scales) oscillations, and of high H values for a series with a large fraction of variance at low frequencies (large scales). In line with these expectations, low H values were obtained for hydrological cycle components with small power at high scales and vice versa. In particular, the DFA Hurst parameter estimates ($\hat{H}$) for the Striegis River are 0.52 for the catchment precipitation, 0.08 for evapotranspiration, 0.54 for soil water content, 0.50 for percolation, 0.51 for direct flow, 0.65 for base flow, 0.63 for simulated total flow, and 0.62 for observed flow. Obviously, "persistence" of the Striegis River flows (H>0.5) is linked to the slowly-varying temporal variability of the baseflow.

In addition to the spectral properties of the hydrological cycle components, the general question addressed within this part of the study is whether the SWAT model can reproduce the low-frequency modes detected in the measured Striegis' river flow time series or not. To that avail the SSA-method has been applied. Results of the SSA applied to the measured and simulated streamflow time series, together with the corresponding gGWS's are shown in Figure 4. In this particular case, the main low frequency mode is the ≈ 7 yr. periodicity which explains ≈ 4 % of the time series' joint variability. One may notice that while the annual signal does not seem to be well described by the SWAT-PEST model (Figure 4a vs. Figure 4c), the main simulated low-frequency component is identical with that of the measured data (Figure 4e vs. Figure 4g). This result suggests that the SWAT-PEST model is indeed able to reproduce the low-frequency mode of the studied river flow time series.

Scaling properties of the direct and the baseflow across the Elbe River Basin

The analysis of the streamflow's scaling properties is refined further by separating the direct- and the baseflow component of the 38 daily long-term (1951-2000) streamflow time series measured across the Elbe River Basin. For the baseflow separation the BFI- and the SWAT-BFI algorithms are applied (see also Luo *et al.*, 2012). As shown in Figure 5, the SWAT-BFI method often gives unrealistic, purely mathematical baseflow estimations, wherefore only the results of the classical BFI- method with respect to the scaling properties of the streamflow components will be discussed further. Notice, although the baseflow separation is carried out on the daily flow time series, the Hurst parameter estimation is performed using the corresponding mean monthly values.

The average DFA $\hat{H}$ for the direct, base-, and total flow of the studied series from the Elbe River Basin are 0.58 , 0.72 , and 0.70 , respectively. The latter is qualitatively in line with the "skin effect" discussed above, suggesting that the low-frequency content is often larger for the baseflow than for the total flow. This result also suggests that the DFA $\hat{H} > 0.5$ for the river flow time series is, in this particular case, not an indication of the long-term persistence, but rather an indication of the presence of low-frequency periodic components in the time series themselves (see Hu *et al.*, 2001; Markovic and Koch, 2013).

As Figure 6 illustrates, $\hat{H}$ decreases somewhat with topographic altitude. By relating large $\hat{H}$ with enhanced power at low-frequency scales, Figure 6 alludes to the altitude- dependence of the time series's low-frequency content. Similar results have been found by Shun and Duffy (1999) for a mountainous basin in the western US and have been explained by a filtering effect of volumetric groundwater storage in the mountain rocks and the basin sediments.

As outlined in the theoretical section of the paper, the baseflow recession constant α can be used as an indirect estimator of the aquifer's physical properties and its role in shaping the stream flow spectrum (Eq. 4). Here, the average estimated baseflow recession constant has been estimated as is $\hat{\alpha} = 0.0033$, resulting in an average characteristic aquifer time scale $\hat{t}_c = 248.5$ d. For comparison, Zhang and Schilling (2004) obtained $\hat{t}_c = 760$ d. in the Walnut Creek watershed. As suggested by these authors, when tc $\gg 1$, the aquifer acts as a fractal filter that may take a white noise input signal (H≈0.5) and output a fractal process. Our findings from above appear to corroborate this phenomenon and our next goal is to investigate the connection between H>0.5 of the baseflows and the spectral properties of groundwater head fluctuations. This will be done in the following section by deterministically analyzing the groundwater head fluctuations for various aquifers which, after all, feed the variability of the streamflow and of the baseflow, in particular.

The role of the aquifer during the transport of low-frequency climate signals

Using the MODFLOW (PMWIN) model hypothetical aquifers with characteristics as discussed earlier were simulated. As input recharge to a stream-connected hypothetical aquifer, the percolation (PERC) time series obtained with the SWAT model of the Striegis River Basin described above were used. The nGWS of the PERC time series shown in Figure 7 is dominated by the annual signal, but also alludes to the presence of the ≈ 10.4 yr. periodicity. As discussed above, the DFA $\hat{H}$ of the PERC time series is ≈ 0.5 , indicating a white-noise background spectrum.

The spectra of the simulated hydraulic head fluctuations 150 m away from the stream (Figure 8) indicate a significant amplification of the low-frequency power of the input signal (recharge), but only a negligible power at the annual scale. Moreover, the qualitative agreement with the theoretical formula (Eq. 3) is obvious: an increase of the aquifer's lateral dimension L leads, by virtue of Eq. 6, to an increase in t_c, resulting in a power shift towards lower frequencies. In line with the theoretical formula (Eq. 6), there is a shift to lower frequency-scales with a decrease in the hydraulic conductivity K (Figure 8).

Similar to the behaviour of the power spectra, an increase in the DFA $\hat{H}$ of the monthly hydraulic head fluctuations can be noted when L is increased and K is decreased, (Figure 9). The highest H values ($H = 1.5$) are found for horizontally large, medium-to-low permeable aquifers (see Figures 9c). For all three aquifer types, $\hat{H}$ for the heads decrease with decreasing distance of the groundwater divide from the stream. The average $\hat{H}$ (for all L) of the groundwater heads for sand-, loamy sand- and silt aquifers is 0.80 , 0.91 and 1.0 , respectively. Our numerical experiments with a white-noise recharge, $\hat{t}_c = 250d.$ and specific yield $S_y = 0.25$ resulted in $\hat{H} = 0.8$ for the groundwater head fluctuations (see Eq. 3). For comparison, for a white noise recharge, Zhang and Schilling (2005) reported an average H of 0.53 and 0.42 for the observed and simulate groundwater head fluctuations, respectively. We argue that the differences in the H-estimates between our study and that of Zhang and Schilling is due to the nature of the employed datasets- our simulations extend over a period of approximately 40 years, whereas Zhang and Schilling (2005) had only a 4-year long

record. Consequently, if one keeps in mind all alterations of H and low-frequency power on a long-term "journey" of precipitation through the subsurface compartments of the hydrological cycle, then $H > 0.5$ for the streamflow time series, become less surprising.

CONCLUSIONS

The spectral changes of precipitation through the various stages of the hydrological cycle including precipitation, evapotranspiration, percolation, soil water, direct, baseflow and streamflow have been studied in context of a physically based modeling and stochastic time series analysis. In particular, an automatically calibrated SWAT model has been used to separate the individual hydrological cycle components, whereas the DFA- and the wavelet-methods have been used to evaluate spectral properties of the derived components. The results indicate a spectral shift towards low-frequency scales (≈ 7 yr. and ≈ 10.4 yr. scales) from precipitation to baseflow, paired with an increase of the Hurst parameter from 0.52 for basin precipitation to 0.65 for baseflow. The comparison of the Hurst parameter estimates of the simulated and the measured flows indicates a marginal difference (H=0.63 vs. 0.62), suggesting a good agreement between simulated and observed flows with respect to their stochastic properties. Moreover, the SSA applied to both the measured- and the SWAT-modelled mean monthly flows of the Striegis River reveals a ≈ 7 yr. periodicity as the main low-frequency mode, showing the ability of the SWAT model to reproduce the low-frequency flow variability of the Striegis River.

The analysis of the streamflow's scaling properties has been refined further by analyzing the basic streamflow's components, namely, direct- and baseflow using the SWAT- and the BFI- baseflow separation algorithms. The results from 38 daily long-term (1951-2000) streamflow time series from the Elbe River Basin indicate an inverse relationship between altitude and H parameter value, and larger H values for baseflow than for direct and total flow, namely H=0.72, 0.58, and 0.70, respectively. Furthermore, the average baseflow recession constant and the average characteristic aquifer time scale are estimated to be $\hat{\alpha} = 0.0033$ and $\hat{t}_c = 248.5$, respectively, which is indicative that for a white-noise precipitation, the Elbe River Basin produces fractal baseflow.

The general role of the aquifer in the transport of the low frequency climate signal has been analyzed further by means of the deterministic groundwater flow model MODFLOW. To account for the low-frequency variability observed in the Elbe River Basin, the SWAT-computed recharge in the Striegis River Basin served as input to a hypothetic phreatic stream-connected sand-, loamy sand- and silt aquifer. The results show that there is an increase of the Hurst parameter of the groundwater head fluctuations with both, an increase of the aquifer's lateral dimension L, and an decrease of the hydraulic conductivity (K). A limiting value for H of 1.5 is reached in large-size, medium-to-low permeable aquifers. The average Hurst parameter (for all L) of the groundwater heads is 0.80, 0.91 and 1.0 for sand-, loamy sand- and silt-aquifer, respectively.

Overall, our study has clearly demonstrated differences in the spectral power at the low-frequency interannual to interdecadal scales and in the Hurst parameter estimates for the long-term main hydrological cycle components at the Niederstriegis gage of the Strigis River Basin. We were able to show that a groundwater system has a substantial effect on the increase of Hurst parameter during the water's journey through the hydrological cycle, starting from precipitation and ending at streamflow. Consequently, our results provide some new insight into the sources of the persistence ("Hurst phenomenon") of the streamflows in the Elbe River Basin.

ACKNOWLEDGMENTS

We thank two anonymous referees for comments on the manuscript and the following governmental and scientific institutions for providing us the data: Potsdam Institute for Climate Impact Research (PIK), Deutscher Wetterdienst (DWD), Saxon State Ministry of the Environment and Agriculture (SMUL), The German Federal Institute of Hydrology (BfG), State Office for Environment, Nature Conservation and Geology, Mecklenburg-Western Pomerania (LUNG), Lower Saxony Water Management, Coastal Defence and Nature Conservation Agency (NLWKN), Ministry of Environment, Health and Consumer Protection of the Federal State of Brandenburg (MUGV), State office for flood control and water management of Saxony-Anhalt (LHW), WSA Lauenburg and the WSA Brandenburg. Current research was partially supported by the 7th Framework European program (BIOFRESH, ref. 226874).

REFERENCES

Arnold JG, Allen PM, Muttiah R, Bernhardtand G. 1995. Automated base flow separation and recession analysis techniques. *Ground Water* **33**:1010-1018.

Beran J. 1994. *Statistics for long-memory processes*. Chapman & Hall, New York, NY; 315.

Chiang W-H, Kinzelbah W. 2005. *3D-groundwater modeling with PMWIN: a simulation system for modeling groundwater flow and pollution*. Springer, Berlin.

Dingman LS. 1994. *Physical Hydrology*. Prentice Hall, Englewood Cliffs, NJ.

Doherty J. 2009. *PEST: Model-independent Parameter Estimation*. Watermark Numerical Computing: Brisbane, Australia.

Furey PR. and Gupta VK. 2001. A physically based filter for separating base flow from streamflow time series. *Water Resources Research* **37**:2709-2722.

Gammaitoni L, Hänggi P, Jung P, Marchesoni F. 1998. Stochastic resonance. *Reviews of Modern Physics* **70**: 223-287.

Gelhar LW. 1993. *Stochastic Subsurface Hydrology*, Prentice-Hall: Englewood Cliffs, NJ.

Ghil M, Allen R, Dettinger MD, Ide K, Kondrasov D, Mann ME, Robertson AW, Saunders A, Tian Y, Varadi F, Yiou P. 2002. Advanced spectral methods for climatic time series, *Reviews of Geophysics* **40**: 1-41.

Gilmore M, Yu CX, Rhodes TL, Peebles WA. 2002. Investigation of rescaled range analysis, the Hurst exponent, and long-time correlations in plasma turbulence. *Physics of plasmas* **9**:1312-1317.

Golyandina N, Nekrutkin V, Zhigljavsky N. 2001. *Analysis of Time Series Structure: SSA and related techniques*. Chapman & Hall/CRC, New York, NY.

Harbaugh AW and McDonald MW. 1996. *User's documentation for MODFLOW–96, an update to the U.S. Geological Survey modular finite-difference ground-water flow model*. U.S. Geological Survey Open-File Report 96–485.

HÜK 200. 2005. *Hydrogeologische Übersichtskarte 1 : 200 000*. Sächsisches Landesamt für Umwelt und Geologie, Dresden.

Hu K, Ivanov P, Chen Z, Carpena P, Stanley HE. 2001. Effect of trends on detrended fluctuation analysis. *Physical Review E* **64**: 011114.

IH, Institute of Hydrology.1980. *Low flow studies*: Wallingford, United Kingdom.

Ionita M, Rimbua N, Lohmann G. 2011. Decadal variability of the Elbe River streamflow. *International Journal of Climatology* **31**: 22–30. DOI: 10.1002/joc.2054.

Koch, M. and D. Markovic, A linear System Approach to convert long-term stochastic Precipitation into Streamflow, MODSIM07, International Congress on Modeling and Simulation, Christchurch, New Zealand, December 10-13, 2007.

Koutsoyiannis D. 2005a. Uncertainty, entropy, scaling and hydrological statistics. 1. Marginal distributional properties of hydrological processes and state scaling. *Hydrological Sciences Journal* **50**: 381-404.

Koutsoyiannis D. 2005b. Uncertainty, entropy, scaling and hydrological statistics. 2. Time dependence of hydrological processes and time scaling. *Hydrological Sciences Journal* **50**: 405-426.

Koutsoyiannis D. 2006. A toy model of climatic variability with scaling behaviour. *Journal of Hydrology* **322**:25-48.

Koutsoyiannis D, Yao H, Georgakakos A. 2008. Medium-range flow prediction for the Nile: a comparison of stochastic and deterministic methods. *Hydrological Sciences Journal* **53**:142-164. DOI: 10.1623/hysj.53.1.142.

Koutsoyiannis D. 2011. Hurst-Kolmogorov dynamics and uncertainty. *Journal of the American Water Resources Association* **47**: 481-495. DOI: 10.1111/j.1752-1688.2011.00543.x.

Lohre M, Sibbertsen P, Könning T. 2003. Modeling water flow of the Rhine River using seasonal long memory. *Water Resources Research* **39**: 1132.

Luo Y, Arnold J, Allen P, Chen X. 2012. Baseflow simulation using SWAT model in an inland river basin in Tianshan Mountains, Northwest China. *Hydrology and Earth Systems Sciences***16**, 1259–1267. DOI:10.5194/hess-16-1259-2012.

Markonis Y, Koutsoyiannis D, Climatic Variability Over Time Scales Spanning Nine Orders of Magnitude: Connecting Milankovitch Cycles with Hurst–Kolmogorov Dynamics. *Surveys in Geophysics* **34**:181–207. DOI 10.1007/s10712-012-9208-9.

Markovic D and Koch M. 2005. Sensitivity of Hurst parameter estimation to periodic signals in time series and filtering approaches. *Geophysical Research Letters* **32**: L17401. DOI:10.1029/2005GL024069.

Markovic D and Koch M. 2013. Long-term variations and temporal scaling of hydroclimatic time series with focus on the German part of the Elbe River Basin. *Hydrological Processes*. DOI: 10.1002/hyp.9783.

Milly PCD and Wetharald RT. 2002. Macroscale water fluxes, 3. Effects of land processes on variability of monthly river streamflow. *Water Resources Research* **38**: 1235. DOI:10.1029/2001WR000761.

Montanari A, Taqqu S, Teverovsky V. 1999. Estimating Long-Range Dependence in the Presence of Periodicity: An empirical Study. *Mathematical and Computer Modeling* **29**: 217-228.

Montanari A. 2003. Long-Range Dependence in Hydrology. In *Theory and applications of long-range dependence*, P. Doukhan, G. Oppenheim, M.S. Taqqu (Eds.). Birkhauser; 461-472.

Neitsch SL, Arnold JG, Kiniry JR, Williams JR. 2011. Soil and Water Assesment Tool, Theoretical documentation, *Texas Water Resources Institute Technical Report No. 406*, Texas A&M University System, College Station, TX.

Peng CK, Buldyrev SV, Havlin S, Simons M, Stanley HE, Goldberger AL. 1994. Mosaic organization of DNA nucleotides. *Physical Review E* **49**:1685.

Richards LA. 1931. Capillary conduction of liquids through porous media .*Physics* **1**: 318–333.

Rorabaugh MI. 1964. Estimating changes in bank storage and ground-water contribution to streamflow. *International Association of Scientific Hydrology Publication* **63**: 432–441.

Schilling KE, Zhang YK. 2012. Temporal scaling of groundwater level fluctuations near a stream. *Ground Water* **50**:59-67. DOI: 10.1111/j.1745-6584.2011.00804.x.

Shun T, Duffy CJ. 1999. Low-frequency oscillations in precipitation, temperature, and runoff on a west facing mountain front: A hydrogeologic interpretation. *Water Resources Research* **35**: 191-201.

Singh VP. 1992. *Elementary Hydrology*. Prentice-Hall, Englwood Cliffs, NJ

Sloto RA and Crouse MY. 1996. HYSEP: A computer program for steramflow hydrograph separation and analysis. U.S. geological survey, Water-Resources Investigations Report

96-4040.
Smith MB, Koren VA, Zhang Z, Reed SM, Pan J.-J. and Moreda F. 2004. Runoff response to spatial variability in precipitation: an analysis of observed data. *Journal of Hydrology* 298: 267-286.
Tikhonov AN and Samarski AA. 1960. *Equations of Mathematical Physics*. Springer, Berlin.
Torrence C and Compo GP. 1998. A practical guide to wavelet analysis. *Bulletin of the American Meteorological Society* **79**: 62-78.
Villarini G, Serinaldi F, Smith JA, Krajewski WF. 2009. On the stationarity of annual flood peaks in the continental United States during the 20th century, *Water Resources Research* **45**: W08417. DOI:10.1029/2008WR007645.
Wang Y and Brubaker K. 2013. Implementing a nonlinear groundwater module in the soil and water assessment tool (SWAT). *Hydrological Processes*. DOI: 10.1002/hyp.9893.
White K and Chaubey I. 2005. Sensitivity Analysis, Calibration, and Validations for a Multisite and Multivariable SWAT Model. *Journal of the American Water Resources Association* 41:1077-1089.
Zhang Y and Schilling K. 2004. Temporal scaling of hydraulic head and river base flow and its implication for groundwater recharge. *Water Resources Research* **40**:W03504. DOI:10.1029/2003WR002094.
Zhang Y and Li Z. 2005. Temporal scaling of hydraulic head fluctuations: Nonstationary spectral analyses and numerical simulations. *Water Resources Research* **41**:W07031. DOI:10.1029/2004WR003797.

FIGURE CAPTIONS

Figure 1. The German part of the Elbe River Basin and the Striegis River sub-basin with the corresponding outlets and climate gages.

Figure 2. Mean monthly Striegis River flows at gage Niederstriegis: measured flows (black line), simulated flows (green line).

Figure 3. Normalized global wavelet spectra of the hydrological cycle components for the Striegis River Basin: precipitation (Prec), actual evapotraspiration (ET), soil water content (SW), groundwater percolation (Perc), direct flow (Sq), baseflow (Gq), total flow at the basin outlet-Niederstriegis (Q). σ^2 and σ_0^2 denote the variance at the particular scale and the time series variance, respectively.

Figure 4. The first three SSA variability modes (first and third column) and the corresponding nGWS's (second and fourth column) of the measured (left two columns) and simulated (right two columns) mean monthly flows (1953-2000) of the Striegis River at gage Niederstriegis. The components are ordered according to the portion of the total streamflow variance they explain (i.e., the first row corresponds to the main SSA variability mode and so on). The red lines in nGWS plots denote the 95% significance levels determined assuming a red noise background, with σ^2 and σ_0^2 denoting the variance at the particular scale and the time series variance, respectively.

Figure 5. Baseflow separation of the daily flows of the Striegis river at gage Niederstrigis (1953-1963) (black line), using the SWAT-basefow filter program (blue) and the BFI-program (red).

Figure 6. Altitude-dependence of the DFA-*H* parameter estimate of the total streamflow from gauges across the Elbe River Basin (black line), baseflow (grey line/empty square) and direct flow (grey line/filled square). (The baseflow separation is done using the BFI-algorithm).

Figure 7. Global wavelet spectra (solid line) of the estimated groundwater recharge (groundwater percolation from the SWAT model of the Striegis River Basin for the period Jan 1953-Dec 2000) and the corresponding 95% confidence level (red line), assuming a red noise background spectra. σ^2 denotes the variance at the particular scale.

Figure 8. Normalized global wavelet spectra of the estimated groundwater recharge for the period Jan 1953-Dec 2000 (grey line) and of the simulated groundwater levels 150m away from the groundwater divide for the sand- (a), loamy sand- (b) and silt-aquifer (c). Aquifer length is set to L = 200 m (dotted line), L = 400 m (dashed line) and L = 800m (thick line). σ^2 and σ_0^2 denoting the variance at the particular scale and the time series variance, respectively.

Figure 9. DFA-H parameter estimates of the simulated monthly groundwater levels at locations d meters away from the groundwater divide for sand- (red), loamy sand- (green) and silt aquifer (blue). The distance L between the groundwater divide and the stream is a) 200, b) 400m and c) 800m.

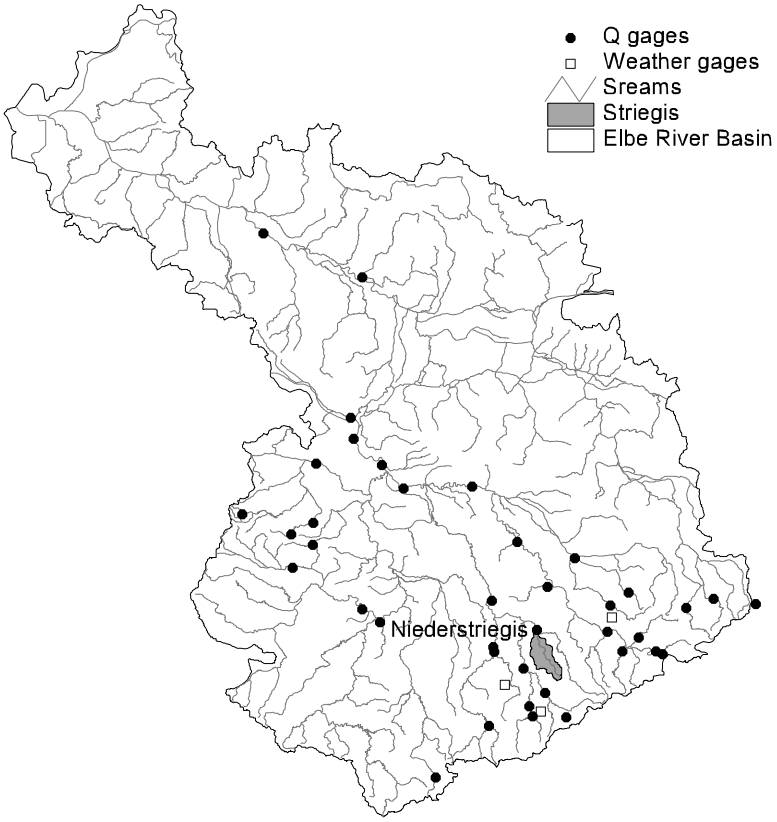

Figure 1. The German part of the Elbe River Basin and the Striegis River sub-basin with the corresponding outlets and climate gages.

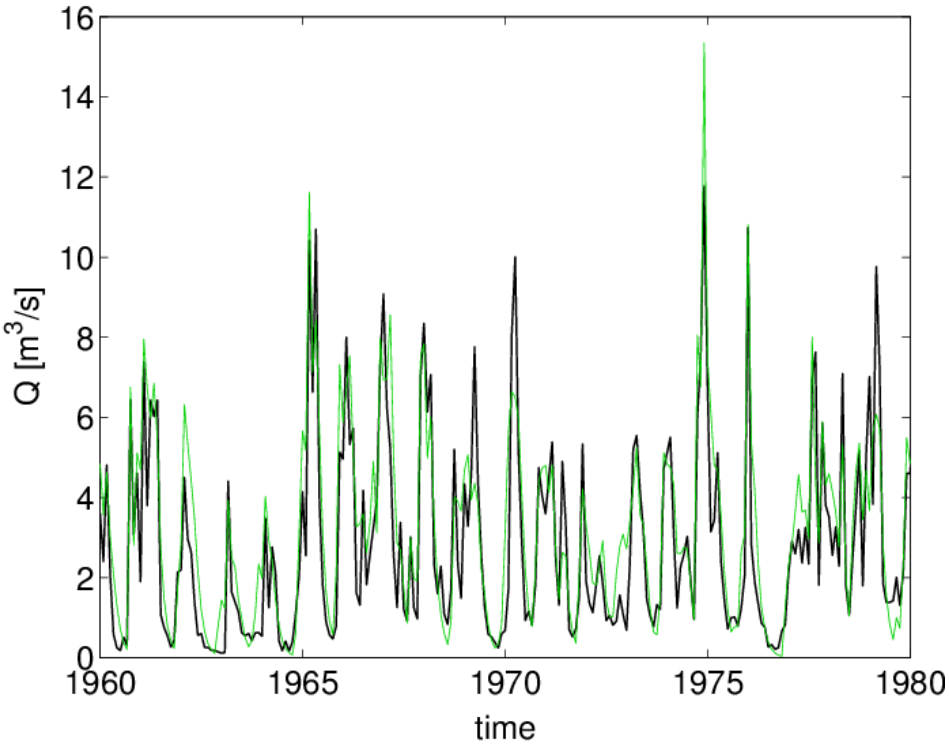

Figure 2. Mean monthly Striegis River flows at gage Niederstriegis: measured flows (black line), simulated flows (green line).

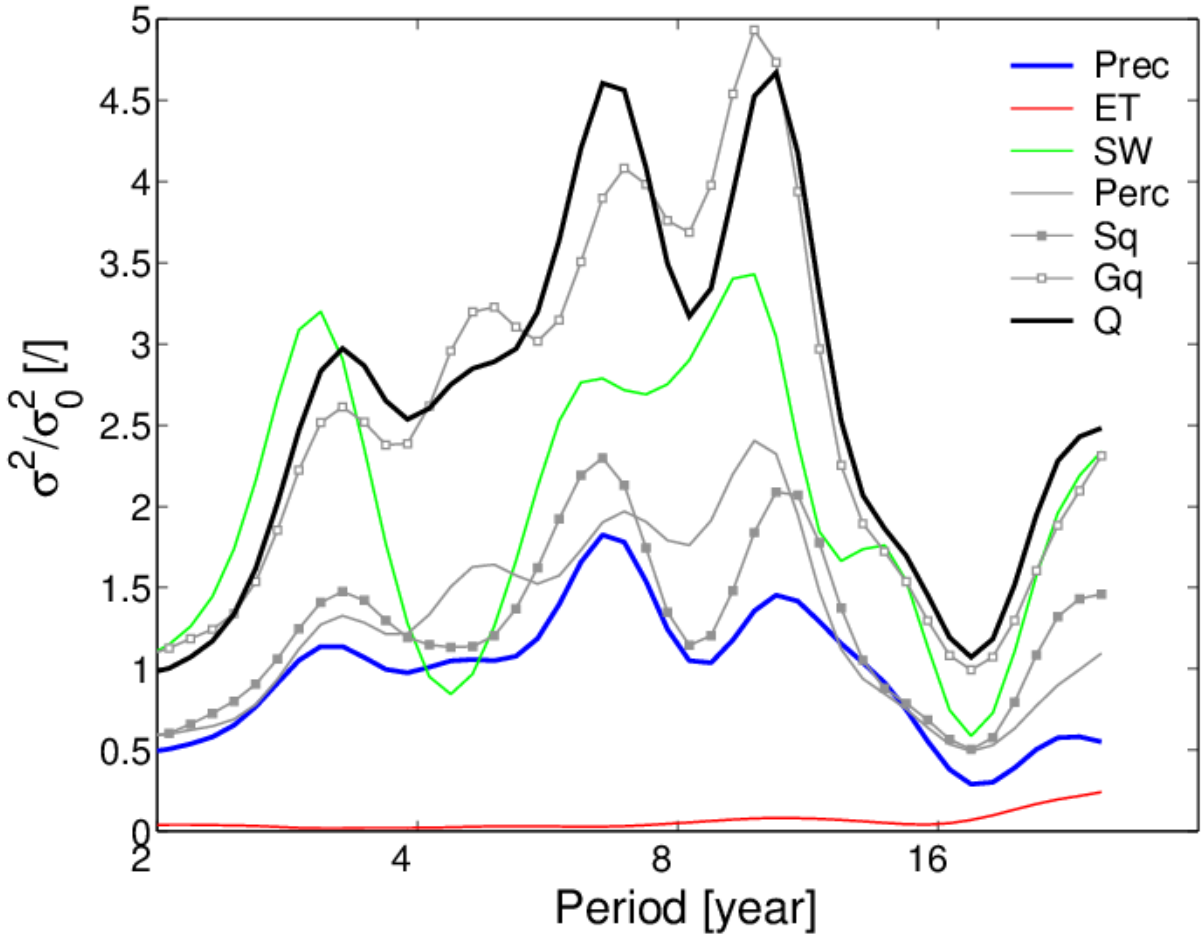

Figure 3. Normalized global wavelet spectra of the hydrological cycle components for the Striegis River Basin: precipitation (Prec), actual evapotraspiration (ET), soil water content (SW), groundwater percolation (Perc), direct flow (Sq), baseflow (Gq), total flow at the basin outlet-Niederstriegis (Q). σ^2 and σ_0^2 denote the variance at the particular scale and the time series variance, respectively.

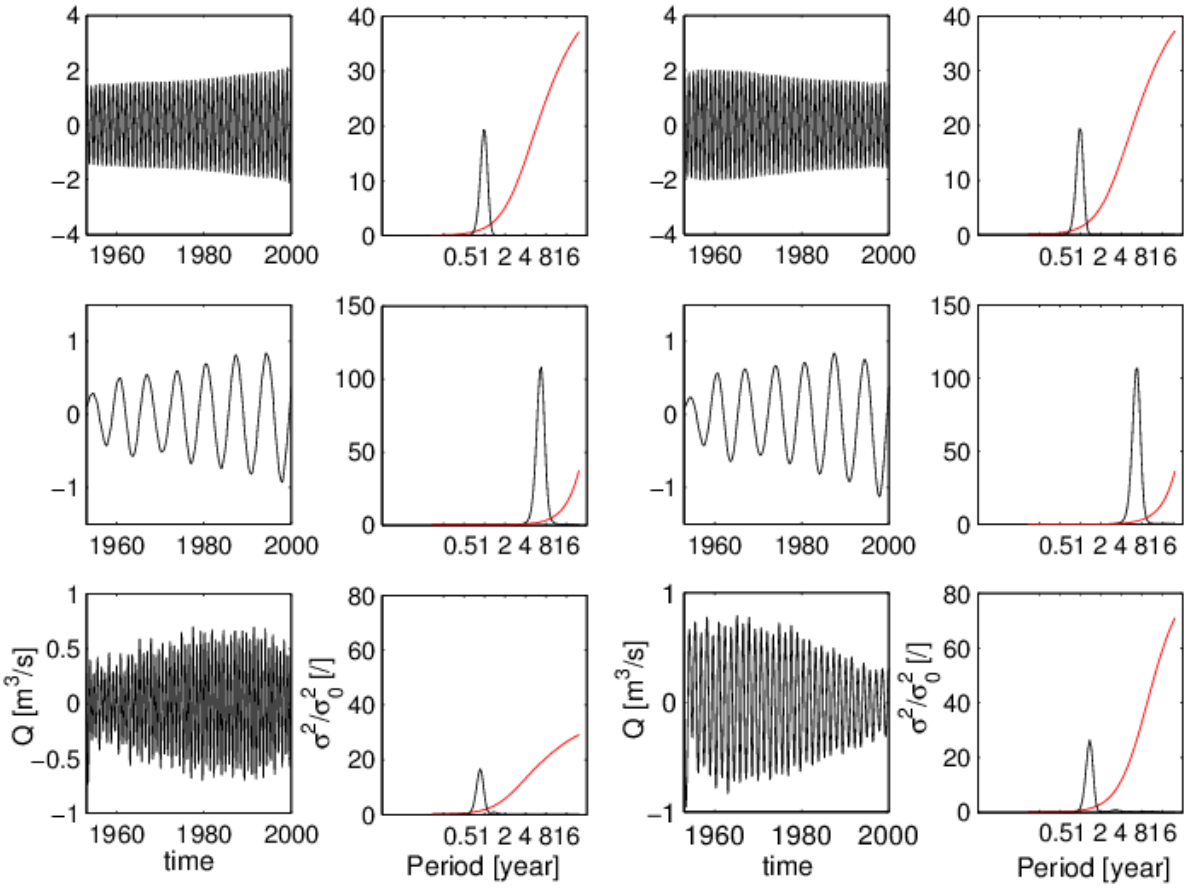

Figure 4. The first three SSA variability modes (first and third column) and the corresponding nGWS's (second and fourth column) of the measured (left two columns) and simulated (right two columns) mean monthly flows (1953-2000) of the Striegis River at gage Niederstriegis. The components are ordered according to the portion of the total streamflow variance they explain (i.e., the first row corresponds to the major SSA variability mode and so on). The red lines in nGWS plots denote the 95% significance levels determined assuming a red noise background, with σ^2 and σ_0^2 denoting the variance at the particular scale and the time series variance, respectively.

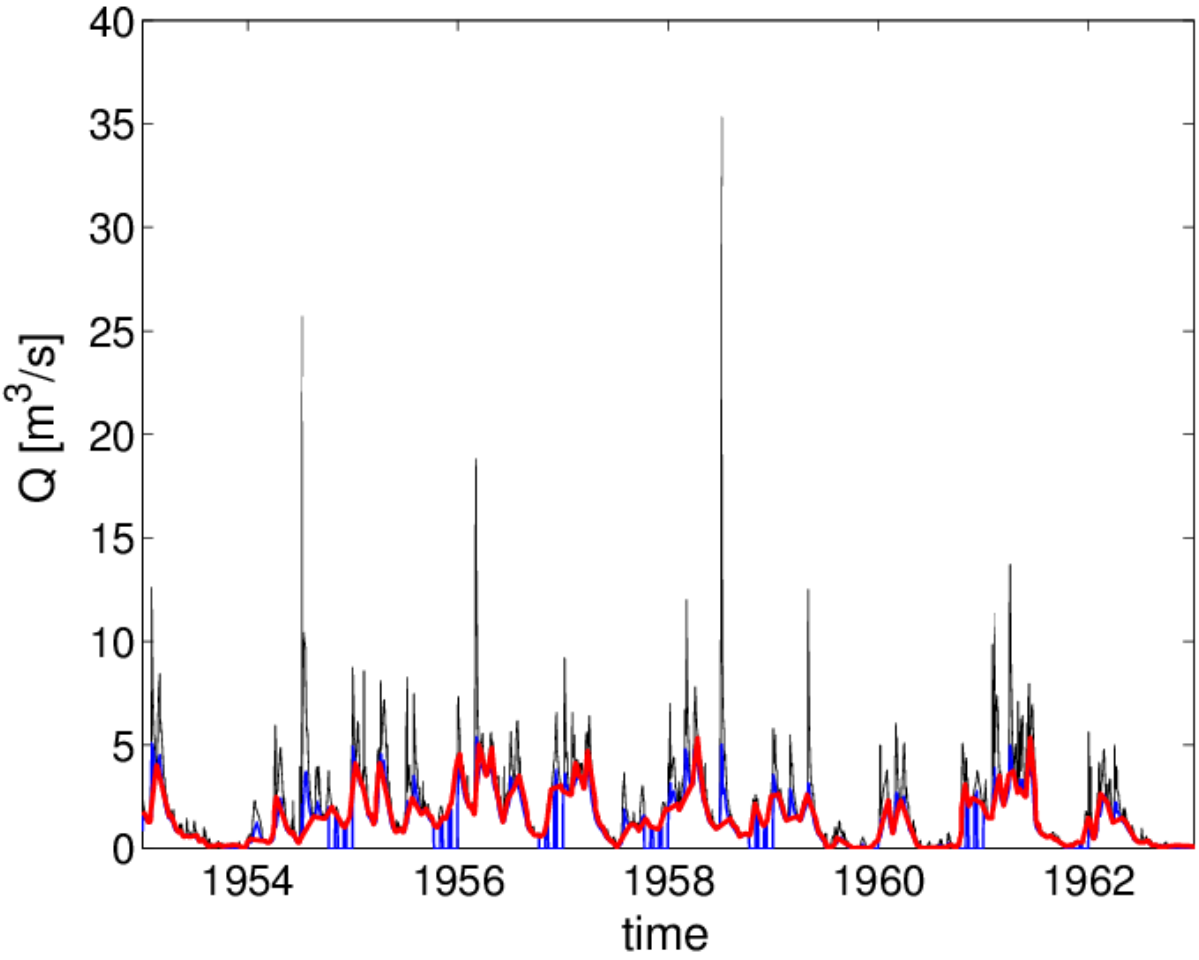

Figure 5. Baseflow separation of the daily flows of the Striegis river at gage Niederstrigis (1953-1963) (black line), using the SWAT-basefow filter program (blue) and the BFI-program (red).

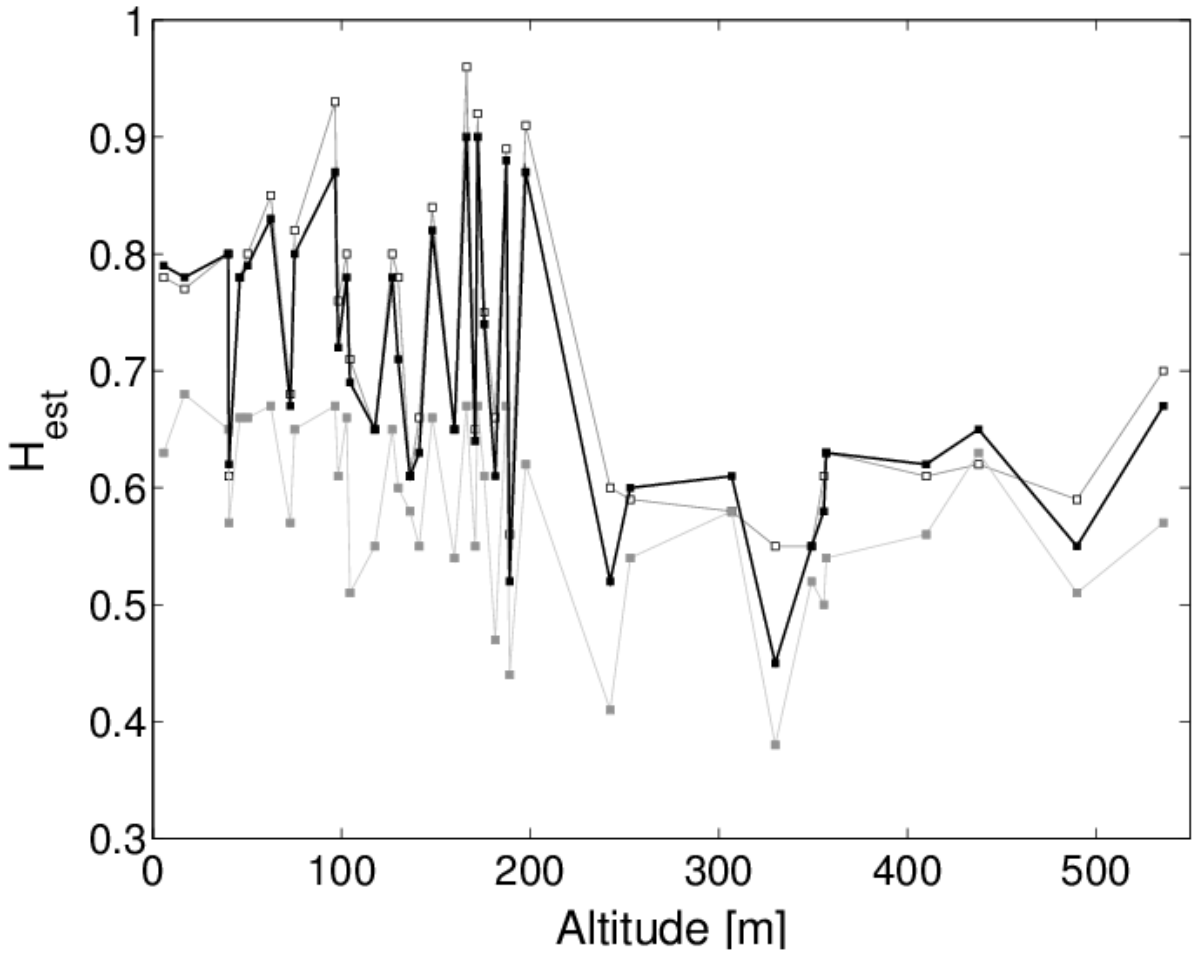

Figure 6. Altitude-dependence of the DFA-H parameter estimate of the total streamflow from gauges across the Elbe River Basin (black line), baseflow (grey line/empty square) and direct flow (grey line/filled square). (The baseflow separation is done using the BFI-algorithm).

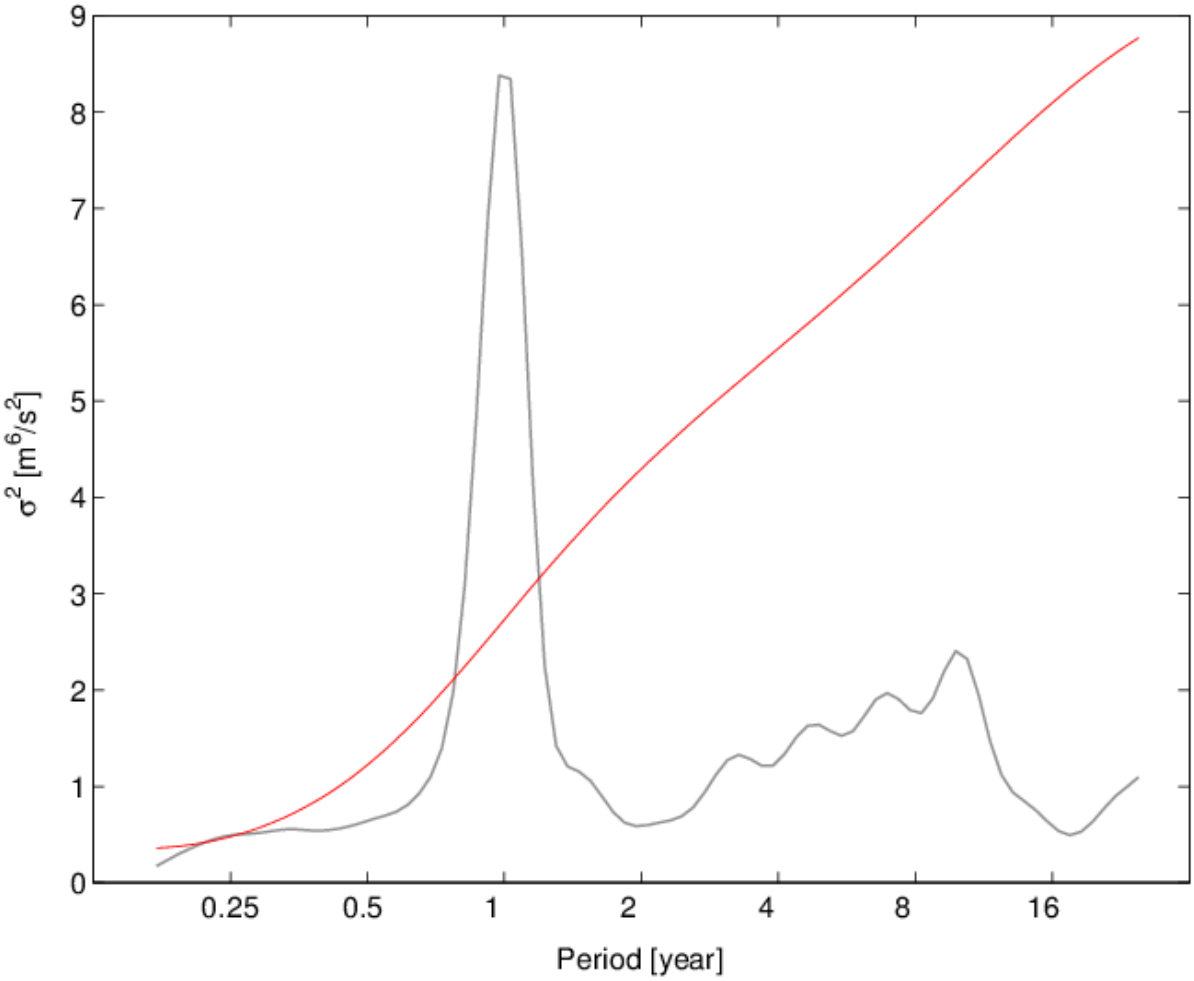

Figure 7. Global wavelet spectra (solid line) of the estimated groundwater recharge (groundwater percolation from the SWAT model of the Striegis River Basin for the period Jan 1953-Dec 2000) and the corresponding 95% confidence level (red line), assuming a red noise background spectra. σ^2 denotes the variance at the particular scale.

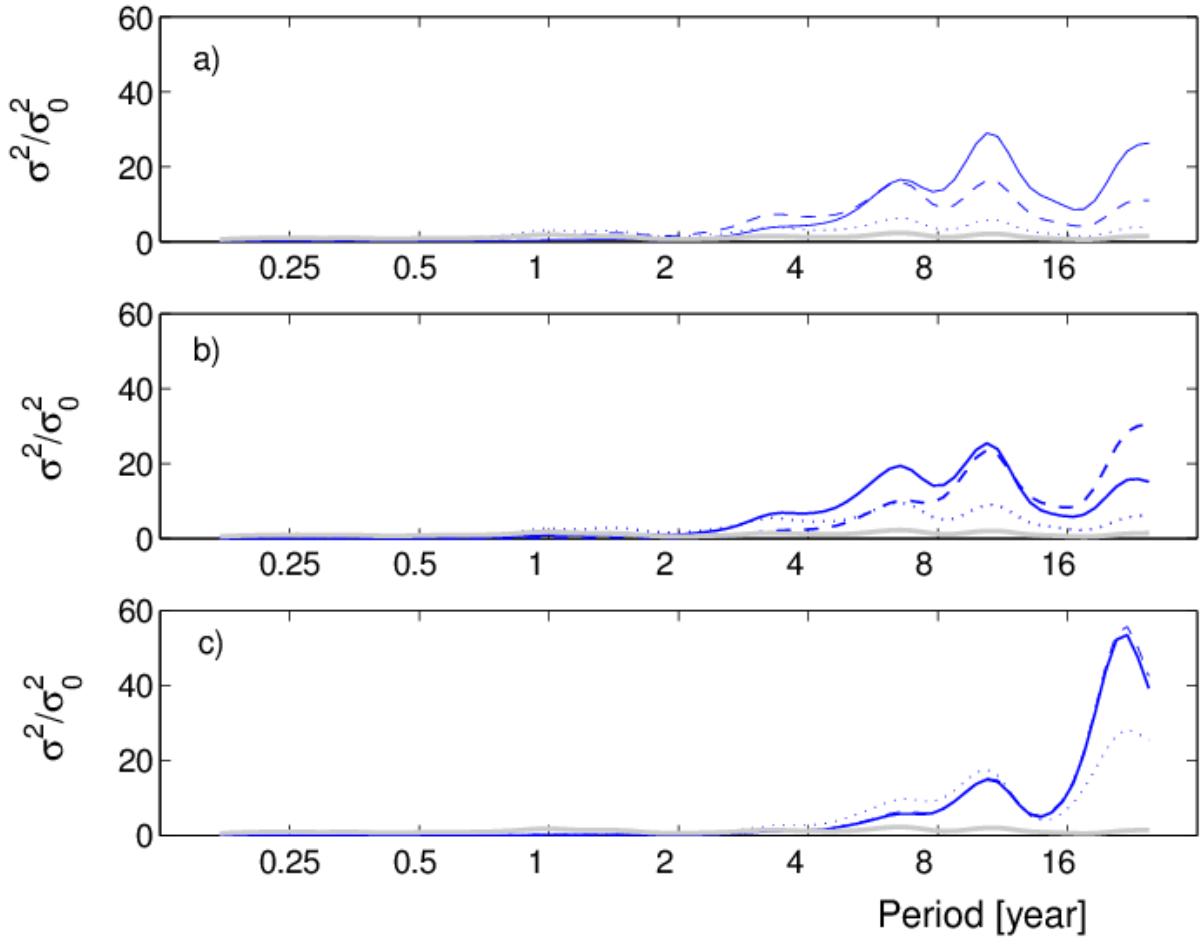

Figure 8. Normalized global wavelet spectra of the estimated groundwater recharge for the period Jan 1953-Dec 2000 (grey line) and of the simulated groundwater levels 150m away from the groundwater divide for the sand- (a), loamy sand- (b) and silt-aquifer (c). Aquifer length is set to L = 200 m (dotted line), L = 400 m (dashed line) and L = 800m (thick line). σ^2 and σ_0^2 denoting the variance at the particular scale and the time series variance, respectively.

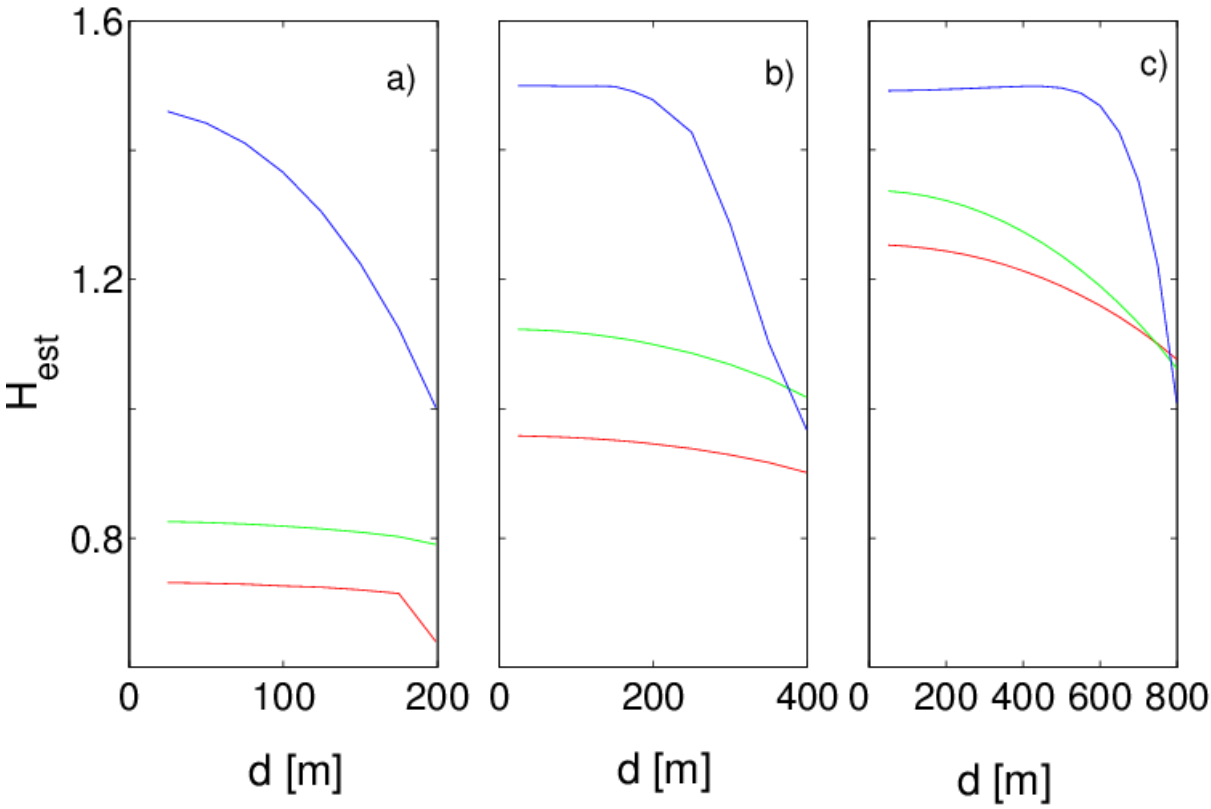

Figure 9. DFA-H parameter estimates of the simulated monthly groundwater levels at locations *d* meters away from the groundwater divide for sand- (red), loamy sand- (green) and silt aquifer (blue). The distance *L* between the groundwater divide and the stream is a) 200, b) 400m and c) 800m.

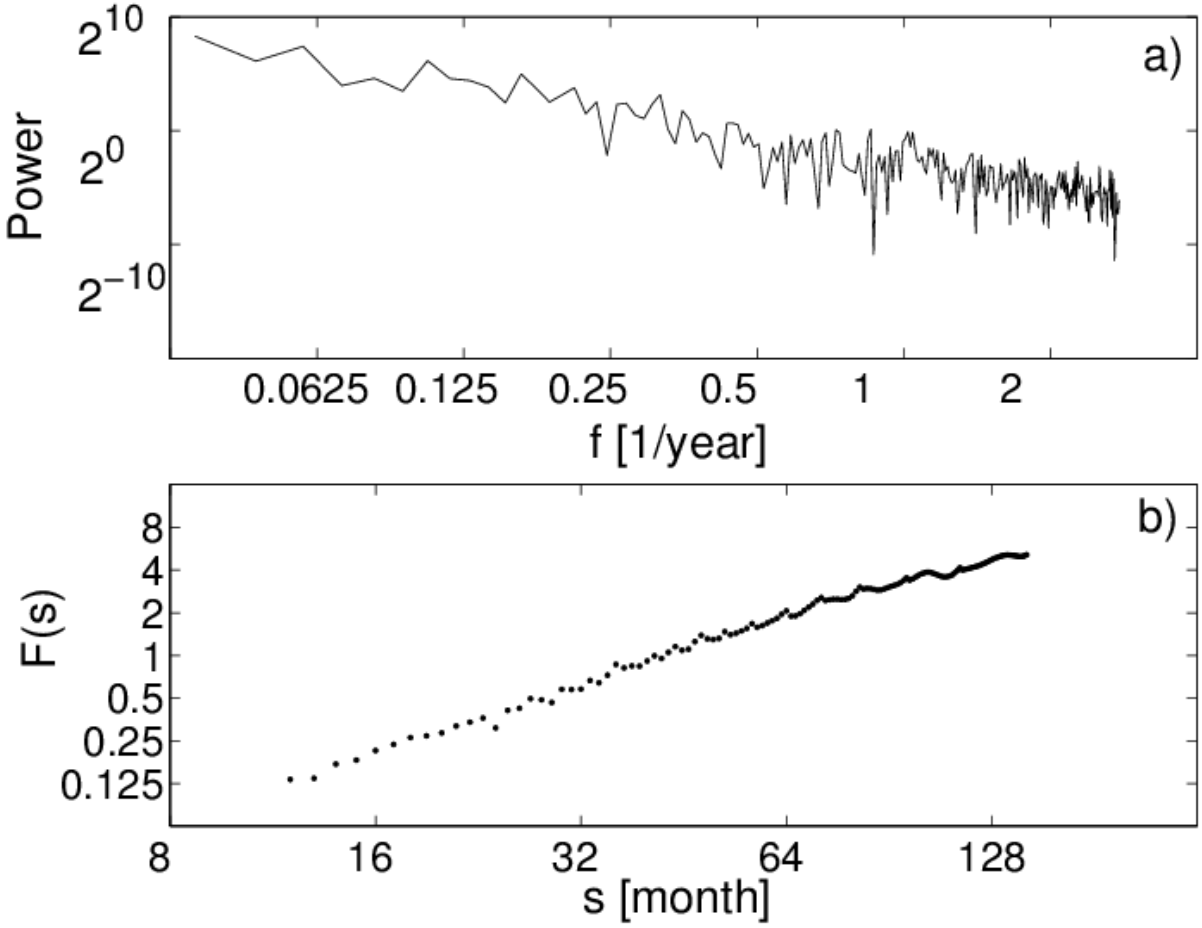

Figure 10. Scaling properties of the simulated groundwater levels in a silt aquifer (L=800m), 150m away from the groundwater divide: a) power spectrum as a function of frequency f ($\hat{\beta} \approx 2$); b) DFA-fluctuation function as a function of scale s, resulting in $\hat{H} \approx 1.5$